Journal of Colloid and Interface Science 384 (2012) 207–216

Contents lists available at SciVerse ScienceDirect

Journal of Colloid and Interface Science

www.elsevier.com/locate/jcis

Colloidal interactions between monoclonal antibodies in aqueous solutions

Dejan Arzenšek [a,b,c,*], Drago Kuzman [a], Rudolf Podgornik [c,d]

[a] Sandoz Biopharmaceuticals Mengeš, Lek Pharmaceuticals d.d., Kolodvorska 27, Mengeš SI-1234, Slovenia
[b] Netica storitve d.o.o., Reteče 97, Škofja Loka SI-4220, Slovenia
[c] Department of physics, Faculty of Mathematics and Physics, University of Ljubljana, Jadranska 19, Ljubljana SI-1000, Slovenia
[d] Department of Theoretical Physics, J. Stefan Institute, Jamova cesta 39, Ljubljana SI-1000, Slovenia

ARTICLE INFO

Article history:
Received 13 April 2012
Accepted 2 June 2012
Available online 28 June 2012

Keywords:
Monoclonal antibody
DLVO theory
Second virial coefficient
Dynamic Light Scattering
Static Light Scattering
Laser Doppler Electrophoresis

ABSTRACT

Colloidal interactions between proteins determine the behavior and stability of globular proteins such as monoclonal antibodies (mAbs) against their propensity to cluster formation in solution. We study interactions between these proteins through their dilute solution behavior. Experiments to quantify intermolecular interactions were done using Dynamic and Static Light Scattering (DLS and SLS) in a high-throughput manner in parallel with zeta potential measurements with Laser Doppler Electrophoresis method (M3-PALS). This approach offers a rapid indirect determination of colloidal interactions through their measured second virial coefficient. Electrostatic part of the DLVO interaction was conveniently parameterized via the corresponding surface charge and/or surface potential, while the van der Waals interactions were parameterized via their Hamaker coefficient, both as functions of ionic strength and pH of the bathing solution. This parametrization of protein–protein interactions improves our understanding of mAb assembly and provides a means for its control by solution parameter variation. Additionally, our results also provide a consistency check and validation of applicability of the DLVO theory in mAbs solution assembly processes.

1. Introduction

Theory of colloidal interactions gives a proper conceptual framework for understanding the solution behavior of globular proteins [1] such as therapeutical monoclonal antibodies (mAbs) [2]. Generally, mAbs as therapeutics are currently gaining tremendous momentum since they are effective at low concentrations with less side effects compared to other small molecule drugs. Due to their charges [3], mAbs can be classified as amphoteric polyelectrolytes. Their net charge can be easily tuned by varying the solution pH past their isoelectric point (IEP). Charged groups are not evenly distributed on the surface of mAbs but rather generate a complex surface mosaic that can make the protein assembly process quite complicated. Furthermore, the occurrence of hydrophilic and hydrophobic groups endows them also with heteropolymer characteristics making their physico-chemical nature highly non-trivial [4] and in many respects drastically different from simple polymeric features.

Globular proteins have a strong propensity to cluster formation or aggregation. In some cases, their aggregation leads to inappropriately formed complexes, which gives rise to inactivation of their therapeutic properties and possible immunogenicity during drug administration [5]. Assembly behavior of mAbs is highly concentration and solution properties dependent, which leads furthermore to very complex phase behavior. The term "protein aggregation" is frequently used to summarize two vastly different phenomena, viz. protein self-association (self-assembly) and protein aggregation proper. Protein self-assembly denotes the formation of small, soluble oligomers, by means of weak non-covalent interactions, that are reversible upon simple dilution in buffer. On the other hand, protein aggregation denotes any irreversible formation of strongly linked aggregates that could be classified as being soluble and/or insoluble and prone to precipitation [6,7].

Protein aggregation can be driven by vastly different mechanisms or processes and eventually leads to crystallization, precipitation, gelation, or liquid–liquid phase separation [8–10]. Random formation of amorphous, visible aggregates defines protein precipitation, whereas ordered three-dimensional lattices define a crystallite as a particular form of protein precipitate. Protein precipitation and crystallization are both assembly processes and better understanding of intermolecular interactions is critical in order to deal with stability issues and crystallization, as well as to elucidate the reason why amorphous precipitates are formed so easily, whereas crystals are not [11].

Protein aggregation depends crucially on inter protein interactions in aqueous solution [1]. Their study is, however, hampered by the fact that it is difficult to experimentally assess the strength and separation dependence of protein–protein interactions in

* Corresponding author at: Sandoz Biopharmaceuticals Mengeš, Lek Pharmaceuticals d.d., Kolodvorska 27, Mengeš SI-1234, Slovenia.
E-mail address: dejan.arzensek@gmail.com (D. Arzenšek).

0021-9797/$ - see front matter © 2012 Elsevier Inc. All rights reserved.
http://dx.doi.org/10.1016/j.jcis.2012.06.055

solution directly as in osmotic stress, surface force apparatus or AFM experiments [12]. What is relatively straightforwardly available is only an indirect determination of inter-protein colloidal interactions via the measurement of their second virial coefficient [13]. In what follows we shall use exactly this approach, coupled to a Derjaguin-Landau-Verwey-Overbeek (DLVO) model [14] of the underlying interaction potential, in order to assess the various parameters entering into the analytical form of this potential.

We will focus on IgG1 monoclonal antibody (mAb) and its interactions in aqueous solutions. The protein used in experiments has the most acute angle observed between the two Fab segments as is evident in 3.2 Å resolution X-ray crystallography [15]. However, it is still too large for its structure to be determined with current NMR methodologies and the structural information obtained from crystal scattering is of limed validity because of the hinge-region flexibility [16].

A three dimensional structure and electrostatic potential surfaces of the whole mAb are presented in Fig. 1 at different pH. At pH 3.0, we can discern a predominance of positive charges and at pH 10.0 a predominance of negative charges. At pH 8.0, which is near IEP of the protein, the positive and negative potentials are evenly distributed. One should note the large positive charge zone at the Fab ends and negative zone in the center of the hinge region. This charge distribution effects the orientational and radial dependence of interactions especially at small separations [17]. In what follows, we will be only interested in the orientationally averaged interactions as they enter the second virial coefficient.

We will use Dynamic and Static Light Scattering (DLS and SLS) in a high-throughput manner as well as concurrent measurements of zeta potential with Laser Doppler Electrophoresis method (M3-PALS) in order to provide as accurate experimental determination of the second virial coefficient as possible and based on this experimental data to parametrize the protein–protein interaction potential in dilute solutions of IgG1 mAb. We will parametrize the repulsive electrostatic component of the protein–protein interaction via the protein effective surface charge and/or its surface potential, while the attractive van der Waals part of the interactions will be parametrized by their Hamaker coefficient. We will study in detail the variation of these parameters with solution pH and ionic strength of a uni–uni valent salt. The goal of this study is thus twofold: to measure the second virial coefficient for this protein and from these experiments extract parameters quantifying the DLVO framework thereby elucidating the range of conditions suitable for its aggregation.

2. Theoretical aspects

Ideally, the behavior of colloidal particles in aqueous solutions may be characterized and quantified within the framework of the DLVO theory [14]. To describe the solution behavior of proteins, we have to take into account the complex protein structure, which complicates the simple DLVO *Ansatz*. Proteins often display poorly understood assembly behavior, which need not correspond neatly to the van der Waals-electrostatic interaction DLVO dichotomy, but can be modified essentially by the presence of non-DLVO interactions such as hydration, hydrophobic, and steric interactions [23].

The electrostatic part of the DLVO theory, the *s.c.* Poisson–Boltzmann electrostatic interactions, predicts repulsion between like-charged colloidal spheres in an electrolyte solution at moderate salt concentrations [12]. The universal attractive part, due to van der Waals interactions [24], represents the long(er) ranged part of the total interaction potential. This picture applies to the equilibrium part of the interaction that bypasses the hydrodynamic and Brownian forces [1]. In the non-equilibrium case, however, the limitations of the pure DLVO theory have to be assessed and hydrodynamic aspects have to be included in an appropriate way, making the understanding of even simple dynamic experiments quite complicated [25].

In the equilibrium case, the model interaction potential, or more appropriately the potential of mean force (PMF), is related to thermodynamics via the second virial coefficient B_{22}, which is frequently used for characterization of pairwise protein self-interactions [13]. By definition, the second virial coefficient reflects the magnitude and direction of the deviations of protein solution from ideality in such a way that positive values of B_{22} indicate net mutual repulsive interactions, and negative values of B_{22} indicate a net protein–protein attraction. The connection is however rather indirect since the second virial coefficient is proportional to an integral of the interaction potential over all separations.

The general variation of the second virial coefficient with solution parameters entails also a small range of slightly negative values, which is usually referred to as the "crystallization slot" because it is closely related to protein crystallization [26]. This range reflects weak attractive interactions conducive to self-association or crystal growth, but it cannot by itself provide a quantitative explanation since kinetic and non-equilibrium considerations should be invoked in order to understand the assembly process [11].

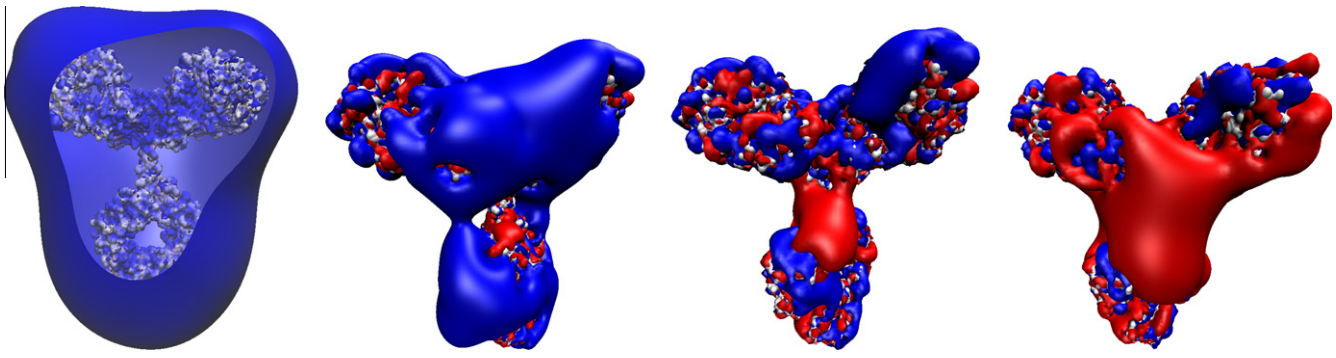

Fig. 1. A three-dimensional representation of the electrostatic potential of a IgG1 monoclonal antibody. The protein structure was constructed using Swiss-PdbViewer [18] and the electrostatic potential was calculated using PDB2PQR with PROPKA pKa prediction [19,20] for preparation of files to compute potential with APBS [21]. Graphical representation was produced using the VMD software [22]. Electrostatic potential contours were calculated (left to right) for pH 3.0, 5.0, 8.0 and 10.0, where red surfaces indicate the −1 and blue the +1 k_BT/e electrostatic potential contours. (For interpretation of the references to colour in this figure legend, the reader is referred to the web version of this article.)

2.1. DLVO interaction model

Within DLVO, the total PMF is given by the sum of repulsive double layer interaction potential between like charges, W_R, and the attractive van der Waals interaction potential, W_A, as [27–29]

$$W(r) = W_A(r) + W_R(r). \tag{1}$$

Here, r is the center-to-center protein separation, leading to a dimensionless rescaled surface separation,

$$x = r/2a - 1.$$

The bare protein radius, a is associated with the hard sphere diameter as $\sigma = 2a$. In Eq. (1), we omitted hydration, hydrophobic, and some unclear short-ranged site specific interactions [23]. We also assumed that the interaction depends solely on the mutual separation of the proteins. For assymmetric particles (see Fig. 1), the repulsive steric or hydration forces are also orientation-dependent, reflecting their shape, and this is usually the dominating factor in determining how molecules mutually align themselves in solutions [12,13,15,30].

The charging of a protein surface in a solvent is due to dissociation of surface dissociable groups [12]. To compute the average electrostatic potential, the ions are described by point charges within the standard Poisson–Boltzmann (PB) approximation [12]. The neglect of finite size of the ions is to some degree permissible in dilute solutions, where the extent of the diffuse layer is considerable, but becomes incorrect in more concentrated electrolyte solutions [31].

The interaction potential, for two weakly charged proteins modeled as spheres with radius a, can be approximated by the Debye–Hückel solution in the limit of low surface potential ($\psi_0 \ll k_BT/e$) [12]

$$\frac{W_R(x)}{k_BT} = \frac{z_p^2\lambda_B}{2a(1+\kappa a)^2}\frac{\exp(-2\kappa a x)}{x+1}, \tag{2}$$

where z_p (i.e., the pH-dependent protein valency) is the effective protein charge and $\lambda_B = e^2/4\pi\varepsilon\varepsilon_0 k_BT$ is the Bjerrum length with value of $\lambda_B \simeq 0.7$nm for water at room temperature. The Debye–Hückel screening length λ_{DH} is related to κ as

$$\kappa = 1/\lambda_{DH} = \sqrt{2e^2N_AI/\varepsilon\varepsilon_0 k_BT}. \tag{3}$$

where $I = \frac{1}{2}\sum_i c_i z_i^2$ is the ionic strength, $c_i = n_i^0/N_A$ (N_A is Avogadro's number) is the molar concentration or molarity (units of mol/L) of free ions of valence z_i, n_i^0 the number density of ions of valency z_i in bulk solution, k_B the Boltzmann constant, T the absolute temperature, ε_0 the permittivity of vacuum, ε the dielectric constant of water and e the elementary charge. Eq. (2) is valid only for distances r large compared to κ^{-1}.

An alternative form for the electrostatic interactions is obtained by letting the protein charge adjust to the surface potential. This situation is described via the charge regulation concept as introduced by Parsegian and Ninham [32]. As it turns out, for any surface charge equilibria, the electrostatic interaction is *always* between the constant charge and the constant potential limits. In the latter case, the corresponding interaction potential can be obtained as [33]

$$\frac{W_R(x)}{k_BT} = \frac{\psi_p^2 a}{2\lambda_B}\frac{\exp(-2\kappa a x)}{x+1}, \tag{4}$$

where ψ_p is now the dimensionless surface electrostatic potential, that is, electrostatic potential divided by k_BT/e. Whatever the protein surface charge equilibrium, the electrostatic interaction energy between two proteins in solution will be always between Eqs. (2) and (4).

The attractive part of the DLVO interaction is given by the van der Waals interactions. For two spheres of equal radii a, the unretarded attractive dispersion potential is given by [24,27,34]

$$\frac{W_A(x)}{k_BT} = -\frac{A_H}{12k_BT}F(x) \tag{5}$$

with

$$F(x) = \frac{1}{(x+1)^2} + \frac{1}{x^2+2x} + 2\ln\left(\frac{x^2+2x}{(x+1)^2}\right). \tag{6}$$

Above, A_H is the Hamaker coefficient and characterizes the magnitude of van der Waals interaction. It is given by [24]

$$A_H = \frac{3k_BT}{2}{\sum_{n=0}}'\left(\frac{\epsilon(\imath\omega_n) - \epsilon_w(\imath\omega_n)}{\epsilon(\imath\omega_n) + \epsilon_w(\imath\omega_n)}\right)^2, \tag{7}$$

where $\epsilon(\imath\omega_n), \epsilon_w(\imath\omega_n)$ are the frequency dependent dielectric permittivities for protein and solvent, evaluated at the imaginary Matsubara frequencies. The magnitude of the Hamaker coefficient for two colloidal particles primarily depends on their chemical composition that sets their overall polarizabilities [35] that then determine the Hamaker coefficient [24].

In this study, A_H is a model parameter and is determined from second virial coefficient experimental data. We assume that the main contribution to the second virial coefficient comes from small separations so that the effects of retardation on the Hamaker coefficient need not be included [24].

2.2. Second virial coefficient and its determination

At present, it is not possible to measure the potential of mean force between proteins in solution directly. We have to take recourse to indirect methods such as the second virial coefficient B_{22} determination. The second virial coefficient enters the osmotic pressure virial equation of state as

$$\frac{\Pi(c)}{RT} = \frac{c}{M} + B_{22}c^2 + \cdots, \tag{8}$$

where c is the concentration of the proteins in solution and M is their molecular mass. B_{22} can be obtained experimentally via Static (SLS) or Dynamic Light Scattering (DLS). By its definition, B_{22} represents an average characteristic of the interaction potential,

$$\begin{aligned} B_{22}M^2 &= 2\pi N_A\int_0^\infty \left(1 - e^{-(W_{HC}+W(r))/k_BT}\right)r^2dr \\ &\simeq 2\pi N_A\left(\int_0^{2a} r^2dr + \int_{2a+h_0}^\infty \frac{W(r)}{k_BT}r^2dr\right). \end{aligned} \tag{9}$$

Here, we divided the interaction potential into a hard core (first term), W_{HC}, and a weak soft tail (second term). We assumed the distance of closes approach is $2a + h_0$ and the soft interaction potential $W(r)$ is by assumption sufficiently weak, so that linearization is in order [33]. Here, N_A is the Avogadro number and $W(r)$ is the (orientationally averaged) potential of mean force, Eq. (1), that depends only on the center-to-center protein separation r.

Assuming now the form Eq. (1) with repulsive electrostatic and attractive van der Waals contributions given by Eqs. (2) and (5), corresponding to a fixed surface charge of the protein, we can write B_{22} in the following form

$$\frac{B_{22}M^2}{2\pi N_A(2a)^3} = \left(\frac{1}{3} + \frac{z_p^2\lambda_B(1+2\kappa a)}{8a(\kappa a)^2(1+\kappa a)^2} - \frac{A_H\Gamma_S(h_0/2a)}{12}\right), \tag{10}$$

where we defined the integral $\Gamma_S(h_0/2a)$

$$\Gamma_S(u) = \int_u^\infty F(x)(1+x)^2dx. \tag{11}$$

On the other hand, if we assume a constant surface potential, that is, Eq. (4) for the electrostatic interaction energy, the corresponding expression for the second virial coefficient would be

$$\frac{B_{22}M^2}{2\pi N_A(2a)^3}=\left(\frac{1}{3}+\frac{\psi_p^2 a(1+\kappa a)}{8\lambda_B(\kappa a)^2}-\frac{A_H\Gamma_S(h_0/2a)}{12}\right). \tag{12}$$

The Debye–Hückel part of this expression is the same as calculated by Petsev and Denkov [33]. If $A_H\Gamma_S>4$, there exists a finite positive value of the effective charge z_p at which the second virial coefficient changes sign.

As will become clear in what follows, it is significant to introduce the dimensionless second virial coefficient k_S in the form

$$k_S=\frac{2B_{22}M}{v_{sp}}=\frac{12B_{22}M^2}{2\pi N_A(2a)^3}= =\left(4+\frac{3z_p^2\lambda_B(1+2\kappa a)}{2a(\kappa a)^2(1+\kappa a)^2}-A_H\Gamma_S(h_0/2a)\right), \tag{13}$$

or equivalently for a fixed surface potential

$$k_S=\left(4+\frac{3\psi_p^2 a(1+\kappa a)}{2\lambda_B(\kappa a)^2}-A_H\Gamma_S(h_0/2a)\right), \tag{14}$$

where v_{sp} is the partial specific volume, which can be determined from protein sphere-equivalent volume fraction as $v_{sp}=(4\pi N_A/3M)a^3$. In the case investigated $v_{sp}=0.73\ \mathrm{cm}^3/\mathrm{g}$.

2.2.1. Second virial coefficient via SLS

In the static case, the Rayleigh scattered light intensity of a protein solution relates to the osmotic compressibility and the protein volume fraction, ϕ, through the slope of the static scattering intensity data in a Debye plot [28,36]. In fact

$$\frac{Kc}{R_\theta}=\frac{1}{RT}\left(\frac{\partial\Pi}{\partial c}\right)=\frac{1}{M}+2B_{22}c=\frac{1}{M}(1+k_S\phi), \tag{15}$$

where k_S has been defined in Eq. (13) and the protein concentration was rewritten in terms of the volume fraction as

$$\phi=cv_{sp}.$$

Here, $R_\theta=R(q)$ is the excess Rayleigh ratio [28] that depends on the scattering angle θ through the wave number $q=\frac{4\pi n_0}{\lambda_0}\sin\left(\frac{\theta}{2}\right)$. Furthermore, $K=(2\pi n_0(dn/dc))^2/N_A\lambda_0^4$ is the system specific optical constant, λ_0 is the wavelength of laser incident light, n_0 the solvent refractive index, and (dn/dc) the refractive index increment with protein concentration, where c is the concentration of the protein (in g/ml). R is the molar gas constant ($R=N_Ak_B$).

2.2.2. Second virial coefficient via DLS

To quantify the relation between pairwise protein interactions and protein kinetics, the relation between B_{22} and collective diffusion constant D_c was investigated using Dynamic Light Scattering (DLS). In the following, we limit ourselves to the hydrodynamic regime that pertains to the long wavelength limit and to measurement times long compared to the characteristic time scale of direct non-hydrodynamic interactions [28].

In the hydrodynamic regime, diffusivities derived from DLS are ascribed to the collective diffusion constant D_c. For small volume fractions, one can relate the collective diffusion constant to the solute properties as [37–39]

$$D_c=D_0(1+k_D\phi). \tag{16}$$

Here, k_D may be split into several different contributions and D_0 is the single particle diffusion coefficient related to the hydrodynamic particle radius a (assumed to coincide with the interaction radius) via the Stokes–Einstein relation $D_0=k_BT/6\pi\eta a$, where η is the solvent viscosity.

The interaction parameter k_D accounts for both the direct intermolecular interactions through k_S as well as for the hydrodynamic (Oseen) interactions through k_H as [33,40]

$$k_D=(k_S-k_H). \tag{17}$$

k_H, which characterizes the hydrodynamic interactions, can be obtained in the approximate form [29,40]

$$k_H\simeq k_{H_0}+12\int_{h_0/2a}^{\infty}\mathrm{d}x(1+x)[1-e^{-W(x)/k_BT}]. \tag{18}$$

where k_{H_0} as the hard-sphere contribution and the second term takes into account indirect hydrodynamic interactions [33,35,40]. Decomposing the Oseen contribution to k_D into the hard-sphere and the indirect hydrodynamic interactions due to the soft part of inter-protein interactions [33,35] provides us with a closed form relationship that can then be fitted to the experiment.

In what follows, we used $k_{H_0}=6.44$ [40,29,35] and the second term can be evaluated in the limit of weak interactions in the same way as the second virial coefficient. We obtain

$$k_H=k_{H_0}+\left(\frac{3z_p^2\lambda_B}{a(1+\kappa a)^2(\kappa a)}-A_H\Gamma_H(h_0/2a)\right), \tag{19}$$

for the case of constant surface charge and

$$k_H=k_{H_0}+\left(\frac{3\psi_p^2}{(\kappa\lambda_B)}-A_H\Gamma_H(h_0/2a)\right), \tag{20}$$

for the constant potential case, with

$$\Gamma_H(h_0/2a)=\int_0^{\infty}F(x)(1+x)dx. \tag{21}$$

While SLS is a more sensitive probe of the pair molecular interaction than DLS, the latter provides additional information of particle sizes, as well as assembly kinetic behavior inaccessible to SLS.

3. Light scattering measurement of interactions between proteins

3.1. Materials and sample preparation

The IgG1 monoclonal antibody (mAb) with molecular weight of 145×10^3 g/mol and pI of 8.46 measured by isoelectric focusing (IEF) was obtained from Sandoz Biopharmaceuticals Mengeš as stock solution of 100 mg/mL in histidine hydrochloride buffer at pH 6.0 and used without further purification. The buffer reagents were obtained from Fischer Scientific (Fair Lawn, NJ, USA) and Sigma–Aldrich Chemical (St. Louis, MO, USA). All chemicals used were reagent grade unless specified. Deionized Milli-Q™ grade water was used to prepare all solutions. Buffers glycine hydrochloride (pH 3.0), acetic acid–sodium acetate (pH 4.0, 5.0), histidine hydrochloride (pH 6.0), monosodium phosphate–sodium hydroxide (pH 7.0, 8.0), tris (hydroxymethyl) aminomethane hydrochloride (pH 9.0), and glycine sodium hydroxide (pH 10.0) were prepared to maintain the solution pH. Appropriate buffer concentrations were selected via Henderson–Hasselbalch equation to maintain the low total ionic strength at 15 mM without the addition of NaCl. They were then passed through 0.22 μm Millipore filters (Billerica, MA, USA). For higher ionic strengths, NaCl was added to the total ionic strengths of $I=30$ mM,50 mM,75 mM,100mM, and175 mM. The protein solutions were buffer exchanged to the desired pH using PD MidiTrap G-25 buffer exchange columns in spin protocol (GE Healthcare). Subsequently, the concentration was adjusted to 10 mg/mL in aliquots before centrifugation on Eppendorf minispin

(HA, Germany) mini-centrifuge at 7000*g* for 10 min to settle any dust particles and then stored at ~ -80 °C.

Before analysis, we prepared samples at lower concentrations by dilution with the corresponding buffers adding desired salt concentration with the help of the Tecan robot. The samples were pipetted into Corning microtiter 0.2 μm filter 96 well plate (Corning Incorporated, NY, USA) and centrifuged on Eppendorf centrifuge (HA, Germany) at 2000*g* for 30 min to remove residual dust and air bubbles. Finaly, filtered samples were prepared in Greiner 96(384) well (half-area) UV-transparent flat-bottom microtiter plate (Greiner Bio one, NC, USA) with 100 μL sample volumes and their concentrations were measured with UV absorption measurement (Tecan) at 280 nm (using extinction coefficient $\alpha_{280} = 1.48(\mathrm{mg/mL})^{-1}\ \mathrm{cm}^{-1}$ for 0.1% (w/v) protein solutions) in a temperature-controlled plate reader. Before measurements, the plate was covered and placed in an automated light scattering instrument.

3.2. Methods

DLS and SLS measurements were conducted using a Malvern Instruments Zetasizer APS (the temperature-controlled auto plate sampler), and zeta potential measurements were performed with Malvern Instruments Zetasizer Nano (Worcestershire, UK). All measurements were conducted at 25 ± 0.1 °C. Zetasizer APS automates measurements from samples prepared in industry standard 96- or 384-well plates and a range of concentrations for collection of both dynamic and Static Light Scattering data. It utilizes a $\lambda_0 = 830$ nm (NIR) laser with output power 60 mW and analyses scattered light at an angle of 90°. The solution viscosity varies at the high buffer reagents concentrations and therefore must be corrected. The buffer viscosity estimated with help of Complex solvents builder in Malvern's DTS software was used for calculations. The standard sample we have used is 10% (w/w) sucrose (Sigma–Aldrich Chemical) solution diluted in Milli-Q™ water and filtered with 20 nm Anotop filter (GE Healthcare). This particular concentration of standard sample has been measured in a Malvern's Zetasizer μV beforehand, to establish a Rayleigh ratio by comparing its scattering with that of Toluene. The Rayleigh ratio of standard sample was taken as $R_{\theta=90^\circ} = 2.09 \times 10^{-6}\ \mathrm{cm}^{-1}$ and its standard refractive index of $n_{sucrose} = 1.35$. Protein Rayleigh ratios were determined after subtracting the background signal of the buffer solution. The solvent value of $n_0 = 1.33$ for water and specific refractive index increment for globular proteins of $\mathrm{d}n/\mathrm{d}c = 0.185$ were used for calculation of the optical constant $K = 4.68 \times 10^{-8}\ \mathrm{mol\ cm^2/g^2}$.

We have used an alternative procedure for measuring B_{22} with a DLS instrument that is equipped with an avalanche photodiode (APD) as the scattered intensity signal detector [41]. DLS uses an attenuator, which limits the intensity that reaches the detector and ensures that there is no saturation on APD, in order to set the scattered intensity at the highest sample concentration. This setting of attenuator was then used for lower concentration dilutions where appropriate attenuation of the scattering signal is provided and used to avoid detector saturation. The same samples were measured simultaneously in both SLS and DLS mode. A single nonassociating species was assumed to exist (checked with PdI values), and a combination of assembly states independent of concentration and leading to weak reversible oligomerization was ignored [36]. This is completely consistent also with the low scatter in the molecular weight *M*, see Fig. 3.

For DLS and SLS measurements, a total of 15 scans, with 30 s duration between them, were accumulated for each sample in five replicates and the results averaged to obtain the final result and standard error estimate. Malvern's DTS software was used to analyze the correlogram using a quadratic cumulant expansion analysis [42] to obtain D_c. Data were rejected if the PdI values were greater than 0.09 (values <0.05 indicating narrow size distributions).

For zeta potential measurements, the sample was prepared at low buffer ionic strength and adjusted to a concentration of 1 mg/mL. The measurements were performed with titration from pH 3.0 to pH 9.0. The analysis was performed using a DTS1060 disposable cell with monomodal mode analysis. It involves the fast field reversal technique (FFR) to obtain mean zeta potential. Each measurement was an average of 30 zeta potential measurements, and results were averaged for each five independent replicates at every pH value.

4. Results and discussion

Light scattering experiments were conducted over the pH range of 3–10, with buffer ionic strength due to uni–uni valent NaCl solution between 15 and 175 mM. The scattering intensity data are presented as Debye plots in Fig. 2 and as volume fraction dependent diffusion coefficients D_c vs ϕ at pH 5 for various ionic strengths as codified by the screening parameter κ. The linearity of the Debye plots persists throughout the range of investigated protein concentrations. The concentrations were chosen to be in the linear regime consistent with other experiments [28]. Because the intensity of scattered light is proportional to protein concentration and to the square of protein molecular weight, measurements with high molecular weight components and/or at self-associating behavior in semidilute concentration regime are problematic [41]. This hurdle was circumvented by using an attenuator to limit the scattered intensity on the APD diode. In the future investigations, we plan to extend measurements to the semidilute regime in order to assess the range of linear concentration behavior and to accurately determine molecular weights and possible assembly states. There is also an interest to extract the information about both monomeric and higher-order assembly protein states from B_{22} values [43].

The intersections of linear fits w.r.t the volume fraction in the SLS mode give the molecular weight *M* via Eq. (15) and infinite-dilution diffusion coefficients D_0 via Eq. (16) in the DLS mode. The data do not collapse to a single point, but can depend on electrolyte concentration, type and on solution pH. This is clearly shown in Fig. 3 where the molecular weight *M* and infinite-dilution diffusion coefficients D_0 are presented for each value κ as function of pH. The value of D_0 was used for calculation of radius *a* and consequently for calculation of dimensionless value κa. It was determined as the mean of intercepts at $\kappa = 1.38\ \mathrm{nm}^{-1}$ for each solution pH with value of $D_0 = 4.43 \pm 0.07 \times 10^7\ \mathrm{cm^2/s}$. This value falls into the previously published experimental range of $4.16 - 4.54 \times 10^7\ \mathrm{cm^2/s}$ [44–47]. *M* and D_0 seem to have a slight ionic strength dependence through the dependence on κ and a pronounced dependence on pH. Except for small pH and for pH $\simeq$ 9, the measured *M* agrees nicely with the molecular weight calculated from the primary sequence of the protein, that is, approximately 145×10^3 g/mol.

From Fig. 3, the main variation of *M* and D_0 is given by the solution pH, which would imply changes in the surface charging/adsorption equilibrium either of the mobile ions or possibly the charged impurities in the solution. We also notice a pronounced variation for the lowest values of pH (pH = 3–4) and $\kappa = 0.4\ \mathrm{nm}^{-1}$ that levels off for larger κ. With increasing pH, we also see an increase in D_0 and a decrease in *M* for the smallest value of κ. There is a dip in both dependencies at pH = 8 that we investigate further by determining the sign of the protein charge in the zeta potential measurements. The salt dependence of the diffusion coefficient for highly charged colloidal particles in the limit of

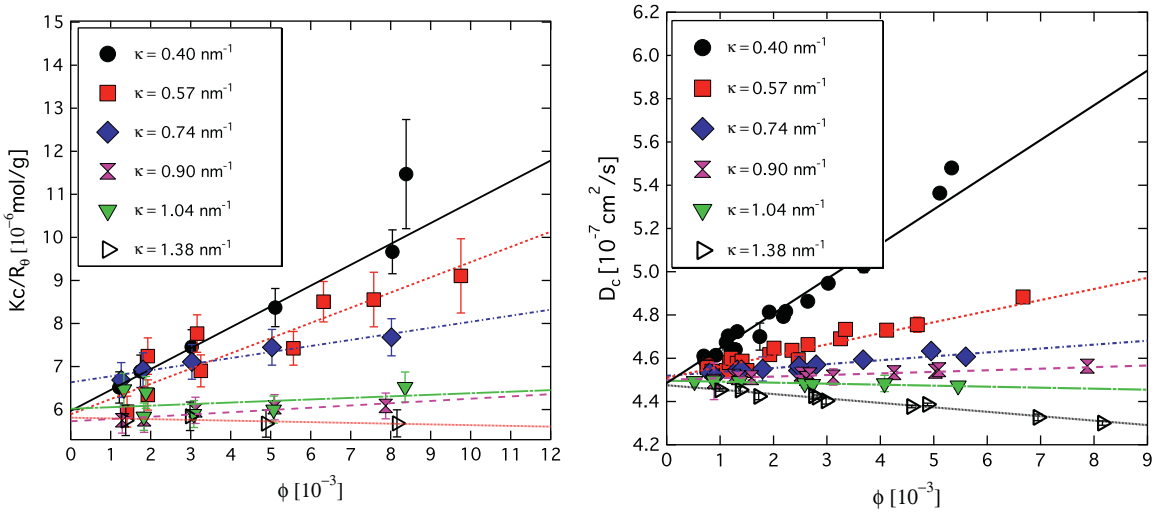

Fig. 2. Debye plots of scattering ratio Kc/R_θ (left) and diffusivities D_c (right), vs protein volume fraction ϕ. pH = 5.0 and different symbols indicate different ionic strengths as codified by their inverse Debye length κ. The error bars in D_c are relatively unnoticeable (usually smaller then the symbol size) when compared to those of Kc/R_θ. Linear fits are obtained using Eq. (15) and (16).

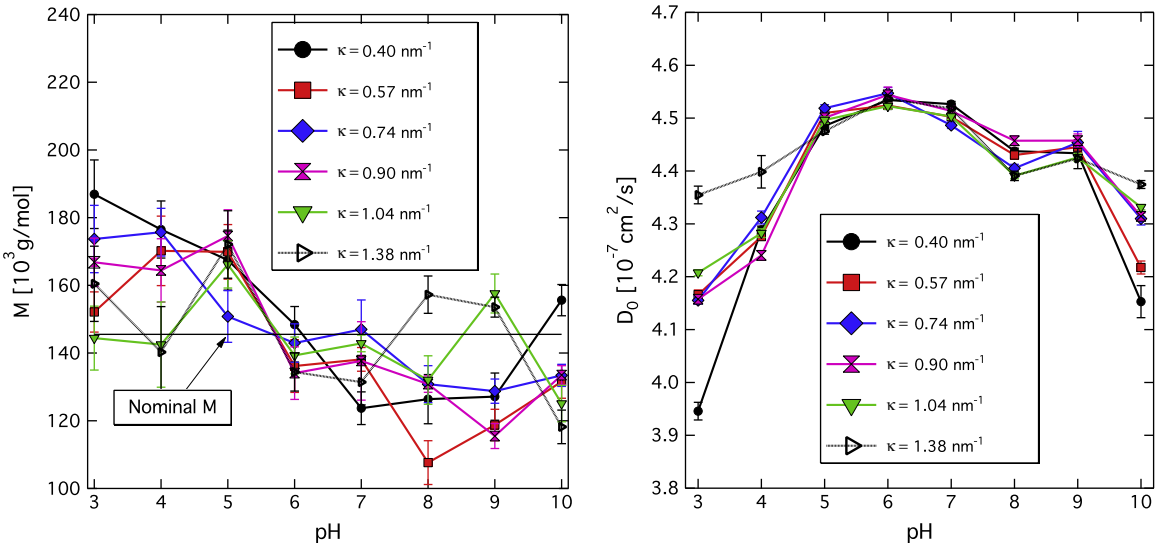

Fig. 3. Molecular weight M (left) and infinite-dilution diffusion coefficient D_0 (right) for each pH at different κ. The lines are shown solely to guide the eyes. Nominal molecular weight calculated from the primary sequence of the protein is obtained as 145×10^3 g/mol and is indicated by a horizontal line in the graph.

constant surface potential was detected and investigated before, see Refs. [33,48,49]. It was shown that D_0 passes through a minimum at $\kappa a \approx 1$ and for $\kappa a \geqslant 3D_0$ coincides with the Stokes–Einstein diffusion coefficient D_{SE}. With similar arguments, we can extract high salt concentration bare hydrodynamic radius by assuming that in this regime $D_0 = D_{SE}$.

The strong effect of solution conditions, Fig. 4, on mAb dimensionless second virial coefficent k_S (SLS) and dimensionless hydrodynamic interaction parameter k_D (DLS) is clearly seen by applying Eqs. (3) and (16) to the analysis of data. The static and dynamic measurements show two trends. For some ionic strengths, k_S shows a non-monotonic behavior, with a region of negative k_S. This first of all indicates that the electrostatic repulsion is screened with the addition of electrolyte to the bathing solution, as well as that the attractive van der Waals interactions can change the overall sign of the second virial coefficient. The details of these trends depend on different ionic strengths of the solution and are most pronounced at low ionic strengths, suggesting that they depend on protein surface charge as well as its sign. As ionic strength increases, the pH dependence gradually levels off. One can clearly observe a trend from positive to negative second virial coefficient at $pH \geqslant 7$ when ionic strength is varied. The possible causes for this dependence lie in the change of sign of the surface charge as the protein has its IEP at 8.46, which is measured without considering the electrical double layer and electrokinetic effects.

The change of sign of the second virial coefficient can be interpreted as an indicator for incipient self-associating behavior and/or possibly the presence of reversible assembly states. With the addition of salt, the repulsive electrostatic interactions are effectively screened and the van der Waals driven association would ensue.

On the other hand, the behavior of the interaction parameter k_D from the DLS data has a much simpler and regular behavior, Fig. 4. On the average, it falls off monotonically with pH for any value of the ionic strength, eventually becoming and staying negative. There is, however, a clear dip in the interaction parameter at the value of pH = 9, which is again very close to the protein IEP value

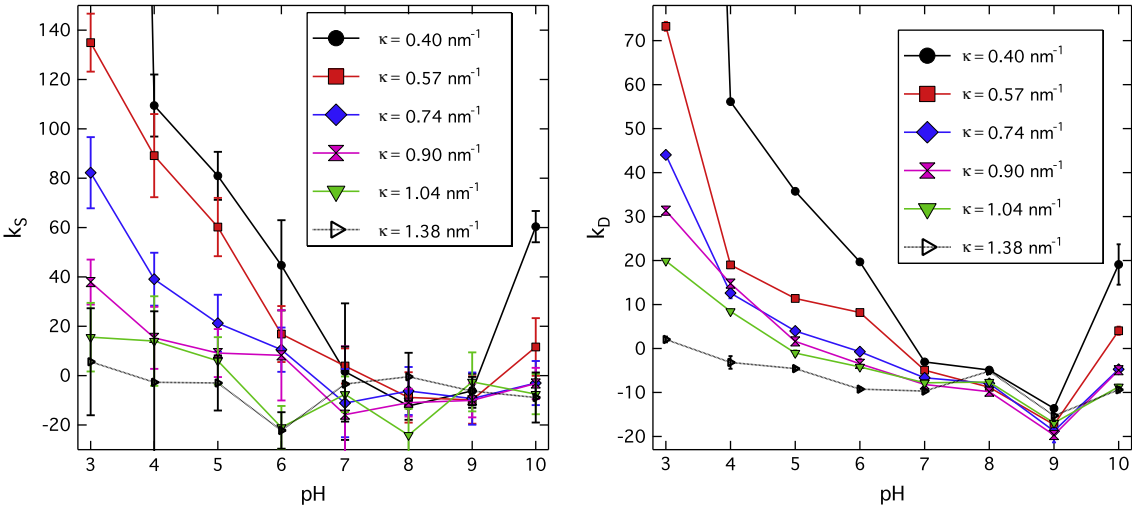

Fig. 4. Parameters k_S (left) and k_D (right) from Eqs. (15) and (16) as a function of solution pH and the ionic screening parameter κ. The lines are shown solely to guide the eyes. The result for pH 3.0 and $\kappa = 0.40\ \mathrm{nm}^{-1}$ with $k_S = 1270.99$ and $k_D = 460.98$ was not plotted since it falls thoroughly out of range compared with other points. The error bars in k_D are relatively unnoticeable when compared to k_S.

of 8.46. This non-monotonic dependence is simply an indication that the charge of the protein changes sign at the IEP. The ionic strength dependence of the interaction parameter at a fixed pH shows only a monotonically decaying behavior.

In order to explain the behavior seen in the regime $pH \geqslant 7$, that is, the diminishment and eventually the change of sign of the second-order virial coefficient, one needs to invoke changes in the effective surface charge driven by the charging equilibrium at the surface. As will be clear when we present also the direct measurement of the effective charge on the protein, the changes in the charging equilibrium at the protein surface eventually lead to a reversal of the sign of the charge. On the other hand, the high positive values of the second virial coefficient for pH = 3.0 at $\kappa = 0.403\ \mathrm{nm}^{-1}$ ($k_S = 1270.99$ and $k_D = 460.98$) are difficult to explain by anomalously high values of the surface charge. In fact, even the maximum chemical charge pertaining to its primary sequence is not enough to explain the values observed. We could rationalize this result by invoking anomalously large scattering from a protein solution in dilute aqueous electrolyte as is observed but not completely understood also in other cases [50].

From the definition, Eq. (17), it is clear that $k_S > k_D$ for any electrolyte concentration at any pH. The direct dependence of k_D on the interaction parameters is then obtained from Eq. (18), which is however based on additional assumptions [40,29], and has a weaker status then the straightforward connection between k_S and the second virial coefficient. We shall next fit both k_S and k_D theoretical expressions, that is, Eqs. (13) and (14) for the former and Eqs. (19) and (20) for the latter, to the experiment and extract the interaction parameters. Rather then dealing with an unknown charge equilibrium at the surface, we will assume the two limiting cases of either a constant surface charge or constant surface potential for the proteins in solution.

On Fig. 5, we present the fits of k_S to the formulas Eq. (14). We fit separately the constant charge and the constant potential cases, Eqs. (13) and (14), giving z_p and ψ_p. The fits for pH 3.0 at low electrolyte concentrations are the worst and suggest there might be some additional features in the DLVO interaction that we did not take into account. The point where k_S changes sign depends on the salt concentration and pH. Generally, the change in the sign of k_S occurs only for sufficiently high pH and this depends strongly on the dissociation equilibria at the protein surface [28].

The calculated values for effective net protein charge and effective surface potential, z_p and ψ_p, as well as the Hamaker coefficient A_H are shown in Figs. 6 and 7. One needs to observe that the fits for the constant charge have in general much better accuracy then in the case of constant potential. The value of the surface potential for small pH also indicates the possible breakdown of the linearized Debye–Hückel solution and the exact values should be taken with caution. The fitted results for the Hamaker coefficient are overall in the range of reasonable values [24]. Though we detect some dependence of the Hamaker coefficient on the pH of the solution, the relative error of the fits is pronounced and when we take it into account the pH effect mostly disappears. There is also more variation in the Hamaker coefficient as measured by DLS when compared to SLS. However, this deviation is also connected with bigger uncertainty in the fits, as can be clearly seen from Fig. 6. The difference between the fitted value of the Hamaker coefficient between the two methods (SLS vs DLS) could be explained by the fact that the DLS data are connected with more theoretical uncertainties of the fitted form of k_D. The theoretical interpretation is much cleaner in the case of SLS.

The effective protein charge z_p or its surface potential ψ_p decrease monotonically with pH up to pH = 8–9. Above this value, the dependency becomes non-monotonic and both start increasing with pH. This non-monotonic dependence is simply an indication that both z_p as well as ψ_p change sign at $\mathrm{pH} \simeq 8$, a hypothesis that we confirm with direct zeta-potential measurements. Expressions for k_S in both limits in fact depend quadratically on charge and/or surface potential, thus precluding the determination of the sign.

The sign reversal of the protein charge can be due to many reasons, but is most probably the effect of the charging equilibrium of the dissociable surface amino acids that depends strongly on pH. The change of sign allows us to estimate the IEP of the whole protein in solution, which seems to be in the vicinity of ≃8, similar to the value found in isoelectric focusing experiments, 8.46. In these fits, we again observe a discrepancy between the fitted values obtained form SLS vs DSL data, for the same reasons as discussed in the case of analogous fits for Hamaker coefficients. Also the relative errors in the estimated charges and potentials are much larger in the latter case.

To check the reliability of the effective protein charge obtained from the SLS and DLS experiments, we also measured the zeta potential independently with an electrophoresis experiment. Zeta

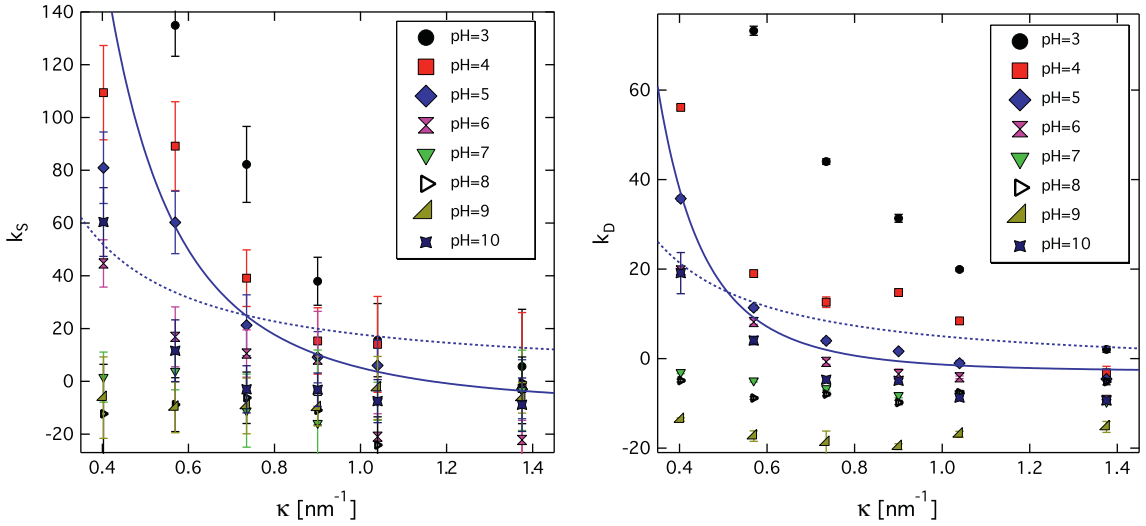

Fig. 5. *Left*: Experimental values for k_S (points) and least square fits to experimental data (lines) vs screening parameter κ for different pH. *Right*: Experimental values for k_D (points) and least square fits to experimental data (lines) vs screening parameter κ for different pH. The value for pH 3.0 at $\kappa = 0.403$ nm^{-1} is not shown because it falls out of range. We show just a single fit for the pH = 5 data in order not to clutter the graph, thus the blue line should due compared with the blue markers. Obviously the fit to fixed charge (thick line) as opposed to fixed potential (dotted line) fares much better. (For interpretation of the references to color in this figure legend, the reader is referred to the web version of this article.)

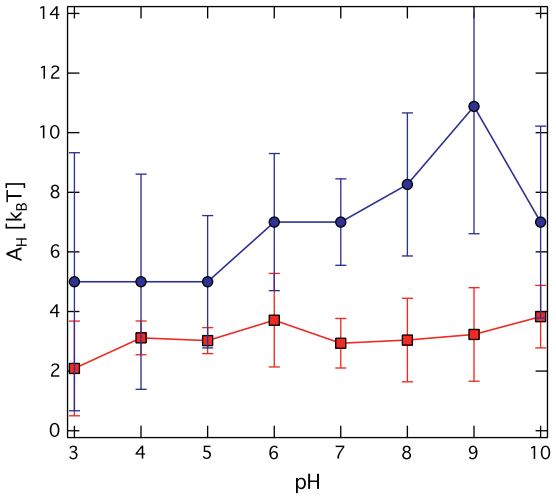

Fig. 6. *Upper graph*: Dynamic Light Scattering. *Lower graph*: Static Light Scattering. Fitted Hamaker coefficient from Fig. 5. The relative error is much larger in the case of DLS then in the case of SLS fits.

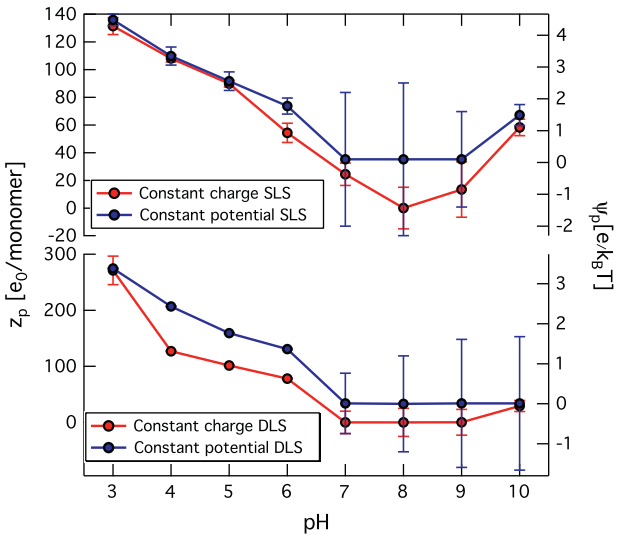

Fig. 7. *Upper graph*: Static Light Scattering. *Lower graph*: Dynamic Light Scattering. Plots of z_p and ψ_p obtained by fitting to experimental data in two different ways: constant charge and constant potential limits. The effective IEP $\simeq 8$ is determined from the zero of the z_p and ψ_p lines. The connection lines are shown to guide the eye.

potential itself then allows to estimate the electrokinetic charge (the protein net charge resulting from zeta potential) and thus the IEP [44]. The zeta potential, ζ, was measured using the Laser Doppler velocimetry technique [51]. The electrophoretic mobility μ_e(m^2/Vs) is measured under an applied potential and converted into ζ (mV) using the Henry's equation [45]

$$\zeta = \frac{3\eta}{2\varepsilon\varepsilon_0 f(\kappa a)}\mu_e, \tag{22}$$

where η is the viscosity and $f(\kappa a)$ is the Henry's function that depends on the particle shape and ionic strength of the medium. For $\kappa a \ll 1, f(\kappa a)$ approaches 1.0 and for $\kappa a \gg 1$, it approaches 1.5. For proteins in this study, assuming a constant radius (a = 5.6 nm), $f(\kappa a) \simeq 1$, regardless of protein concentration and/or solution conditions. The viscosity is obtained from the Einstein relationship assuming that the measured diffusion constant D_0 can be identified as the limit of zero protein concentration.

From the zeta potential ζ, one then needs to calculate the electrokinetic charge z_ζ. There is no single way to do that but depends on the level of approximation one uses for the treatment of solution ions that move with the macroion. For a uniformly charged spherical molecule, the dependence of electrophoretic mobility upon protein valence is given by the linearized Debye–Hückle theory that leads to [44]

$$z_\zeta = \frac{12\pi\varepsilon\varepsilon_0 f(\kappa a)a}{e} \times \zeta. \tag{23}$$

A more accurate formula is obtained by using the full nonlinear Poisson–Boltzmann equation that leads to the following approximate form [49]

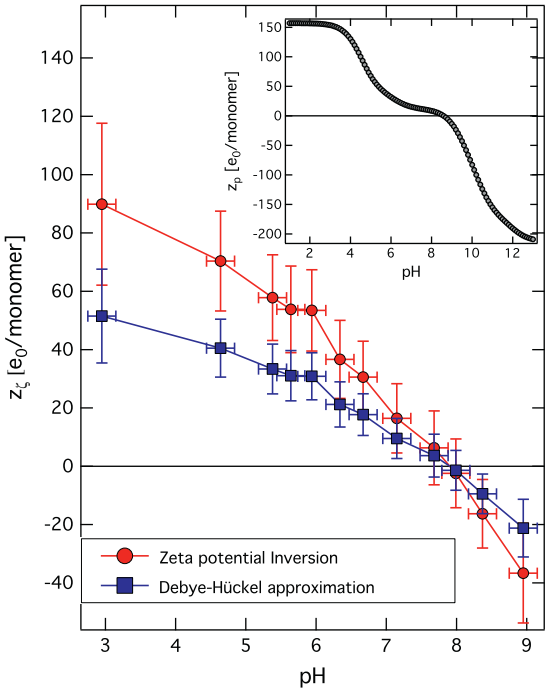

Fig. 8. Charge as calculated from the measured zeta potential and from the primary sequence of AAs (inset). A change of sign is clearly seen. *Red*: calculated from Eq. (24). *Blue*: Debye–Hückel approximation. The inverse Debye length was taken as $\kappa = 1$. The inset shows the theoretical curve obtained form the primary sequence of the mAb sequence with the SEDNTERP utilities available from (http://bitcwiki.sr.unh.edu/index.php/Main_Page). (For interpretation of the references to colour in this figure legend, the reader is referred to the web version of this article.)

$$z_\zeta = (\kappa a)\frac{a}{\lambda_B} \times \left[2\sinh\left(\frac{e\zeta}{2k_BT}\right) + 4\tanh\left(\frac{e\zeta}{4k_BT}\right)\right]. \tag{24}$$

which is accurate to within 5% of the exact value for $\kappa a > 0.5$.

In Fig. 8, we plotted the net charge z_ζ obtained from Eq. (23) as well as from Eq. (24). Both values show similar trends and a similar estimated effective IEP, which is consistent within the limits of error for z_p obtained by fitting the k_S data. The k_D data are further off indicating a less accurate estimate. Nevertheless, there is a pleasing qualitative consistency between all the experimental data on the protein charge variation with pH.

Fig. 8 also shows the theoretical curve obtained form the primary sequence of the protein with the SEDNTERP utilities available from (http://bitcwiki.sr.unh.edu/index.php/MainPage). However, this calculation has other issues as it does not differentiate between the buried amino acids and those on the surface.

The IEP measured by isoelectric focusing is 8.46, which is higher than 7.91 deduced from our experiments. The proteins should be electrically neutral at pH close to IEP, but the value of μ_e is measured at the s.c. shear plane (slipping plane), which separates the thin layer of liquid bound to the solid surface and forms the kinetic unit consisting of moving particles with a certain amount of the surrounding liquid, thus suggesting that binding of counterions results in the difference between the effective IEP and the real value.

5. Conclusions

This study is primarily aimed to measure the second virial coefficient and parametrize it in terms of the net charge, effective Hamaker coefficient, and the IEP of a therapeutical monoclonal antibody IgG1 as probed by different experimental methods. We used Satic Light Scattering, Dynamic Light Scattering, and electrophoretic mobility essay to get the second virial coefficients and zeta potentials of the protein in various solution conditions, spanning the range of $0 < \text{pH} < 10$ and $0.4 < \kappa[\text{nm}^{-1}] < 1.4$. The protein volume fraction in these experiments was within the range $0 < \phi < 10^{-2}$. Our results give a clear insight into the biophysical properties of this protein, which are essential for the interactions in ionic solutions. While the effective charge of the protein controls the repulsive forces between them, the Hamaker coefficient quantifies the strength of the van der Waals interactions. By mapping the solution parameter dependence of both characteristics, we can get a detailed insight into solution conditions appropriate for its aggregation and crystallization.

We found that the effective protein charge as well as the Hamaker coefficient both depend on the solution conditions. The changes in the Hamaker coefficient are bounded and show a much smaller variation for the SLS case then in the DLS case. The Hamaker coefficient is around $3k_BT$ in the SLS case, whereas it shows a steady increase with pH as well as being in general by about a factor of 2 larger in the DLS case. Since the SLS B_{22} data can be interpreted theoretically in a more reliable way, we do not attach any particular importance to the pH variation of the DLS Hamaker coefficient.

There is more quantitative consistency in the effective charge data for the two complementary light scattering methods. Some uncertainty remains in the fitting function for the DLS case where the hydrodynamic effects are taken into account only approximately. In general, the effective charge diminishes with increased pH, reaching the IEP at about $\text{pH} \simeq 8$. The measured changes in the effective charge compare very favorably with those extracted from the zeta potential either in the linear or non-linear limit. The zeta potential experiments also give the IEP of $\text{pH} \simeq 8$. They are consistent with a separate estimate of bare charge based on the complete primary sequence of the protein.

At low pH, the effective charge of the protein is $\simeq +130$, whereas the primary sequence value would be +150. For high values of pH, the charge saturates at $\simeq -30$, whereas the primary sequence value can be as high as $\simeq -200$. From a colloidal point of view for the proteins under consideration, the electrostatic repulsion alone in the DLVO potential apparently provides an accurate description of the solution behavior. This cannot be claimed for some other proteins where the solution stability is mostly determined by water mediated short range interactions [25].

The anomalously large scattering intensity at pH = 3.0 is difficult to explain away and it is not clear at this point whether it is due to anomalous scattering itself, or whether it reflects fundamental changes in the form of the DLVO interaction potential. At this very low values of the solution pH, one could envision a hydration contribution to the interaction potential as has been invoked before to explain anomalies in the second virial coefficient of proteins but not for those values of the solution pH [25].

Parametrization of the protein interactions via the effective charge and the Hamaker coefficient, together with their solution properties variation, gives the potential to control the assembly kinetics. Obviously, the most favorable region in the parameter space for protein aggregation is connected with highest Hamaker coefficient and/or smallest protein effective charge. In the case considered here, this would correspond to the IEP of the protein, as the Hamaker coefficient does not show any pronounced solution parameter variation. Understanding the mechanisms of protein–protein interactions in protein nucleation and growth is necessary for fine tuning the protein assembly dynamics (precipitation or crystallization).

Acknowledgments

This work was financed in part by the European Union, European Social Fund, within the framework of the Operational

Programme for Human Resources Development for the Period 2007–2013. RP acknowledges support of ARRS through research program P1-0055 and research project J1-4297.

References

[1] D. Leckband, S. Sivasankar, Colloids Surf., B 14 (1999) 83.
[2] O. Leavy, Nat. Rev. Immunol. 10 (2010) 297.
[3] H. Mach, S. Gregory, A. Mackiewicz, S. Mittal, A. Lalloo, M. Kirchmeier, M. Shameem, Ther. Deliv. 2 (2011) 727.
[4] A. Finkelstein, O. Ptitsyn, Protein Physics: a Course of Lectures, 1st ed., Academic Press, London–San Diego, 2002.
[5] V. Kayser, N. Chennamsetty, V. Voynov, B. Helk, K. Forrer, B.L. Trout, J. Pharm. Sci. 100 (2011) 2526.
[6] A. Saluja, D. Kalonia, Int. J. Pharm. 358 (2008) 1.
[7] H. Mahler, W. Friess, U. Grauschopf, S. Kiese, J. Pharm. Sci. 98 (2009) 2909.
[8] T. Ahamed, B. Esteban, M. Ottens, G. Van Dedem, L. Van der Wielen, M. Bisschops, A. Lee, C. Pham, J. Thömmes, Biophys. J. 93 (2007) 610.
[9] R. Lewus, P. Darcy, A. Lenhoff, S. Sandler, Biotechnol. Prog. 27 (2011) 280.
[10] A. Dumetz, A. Chockla, E. Kaler, A. Lenhoff, Biophys. J. 94 (2008) 570.
[11] J. Zhang, X. Liu, J. Chem. Phys. 119 (2003) 10972.
[12] J. Israelachvili, Intermolecular and Surface Forces, 3rd ed., Academic Press, 2011.
[13] B. Neal, D. Asthagiri, A. Lenhoff, Biophys. J. 75 (1998) 2469.
[14] E. Verwey, J. Overbeek, K. Van Nes, Theory of the Stability of Lyophobic Colloids: The Interaction of Sol Particles Having an Electric Double Layer, Elsevier, New York, 1948.
[15] L. Harris, E. Skaletsky, A. McPherson, J. Mol. Biol. 275 (1998) 861.
[16] J. Brandt, T. Patapoff, S. Aragon, Biophys. J. 99 (2010) 905.
[17] R. Chari, K. Jerath, A. Badkar, D. Kalonia, Pharm. Res. 26 (2009) 2607.
[18] N. Guex, M. Peitsch, Electrophoresis 18 (1997) 2714.
[19] T. Dolinsky, P. Czodrowski, H. Li, J. Nielsen, J. Jensen, G. Klebe, N. Baker, Nucleic Acids Res. 35 (2007) W522.
[20] H. Li, A. Robertson, J. Jensen, Proteins: Struct., Funct., Bioinf. 61 (2005) 704.
[21] N. Baker, D. Sept, S. Joseph, M. Holst, J. McCammon, Proc. Natl. Acad. Sci. USA 98 (2001) 10037.
[22] W. Humphrey, A. Dalke, K. Schulten, J. Mol. Graphics 14 (1996) 33.
[23] Y. Liang, N. Hilal, P. Langston, V. Starov, Adv. Colloid Interface Sci. 134–135 (2007) 151.
[24] V. Parsegian, Van der Waals forces: A Handbook for Biologists, Chemists, Engineers, and Physicists, first ed., Cambridge University Press, Cambridge, 2005.
[25] D. Petsev, B. Thomas, S. Yau, P. Vekilov, Biophys. J. 78 (2000) 2060.
[26] A. George, W. Wilson, Acta Crystallogr., Sect. D: Biol. Crystallogr. 50 (1994) 361.
[27] R. Curtis, J. Prausnitz, H. Blanch, Biotechnol. Bioeng. 57 (1998) 11.
[28] M. Muschol, F. Rosenberger, J. Chem. Phys. 103 (1995) 10424.
[29] M. Corti, V. Degiorgio, J. Phys. Chem. 85 (1981) 711.
[30] S. Fejer, D. Chakrabarti, D. Wales, Soft Matter 7 (2011) 3553.
[31] D. Ben-Yaakov, D. Andelman, R. Podgornik, D. Harries, Curr. Opin. Colloid Interface Sci. 16 (2011) 542.
[32] B. Ninham, V. Parsegian, J. Theor. Biol. 31 (1971) 405.
[33] D. Petsev, N. Denkov, J. Colloid Interface Sci. 149 (1992) 329.
[34] S. Li, D. Xing, J. Li, J. Biol. Phys. 30 (2004) 313.
[35] D. Kuehner, C. Heyer, C. Rämsch, U. Fornefeld, H. Blanch, J. Prausnitz, Biophys. J. 73 (1997) 3211.
[36] J. Alford, B. Kendrick, J. Carpenter, T. Randolph, Anal. Biochem. 377 (2008) 128.
[37] B. Ackerson, J. Chem. Phys. 69 (1978) 684.
[38] L. Belloni, M. Drifford, P. Turq, J. Phys., Lett. 46 (1985) 207.
[39] P. Prinsen, T. Odijk, J. Chem. Phys. 127 (2007) 115102.
[40] G. Phillies, J. Colloid Interface Sci. 119 (1987) 518.
[41] S. Yadav, T. Scherer, S. Shire, D. Kalonia, Anal. Biochem. 411 (2011) 292.
[42] D. Koppel, J. Chem. Phys. 57 (1972) 4814.
[43] M. Blanco, E. Sahin, Y. Li, C. Roberts, J. Chem. Phys. 134 (2011) 225103.
[44] C. Lehermayr, H. Mahler, K. Mäder, S. Fischer, J. Pharm. Sci. 100 (2011) 2551.
[45] S. Yadav, J. Liu, S. Shire, D. Kalonia, J. Pharm. Sci. 99 (2010) 1152.
[46] S. Yadav, A. Sreedhara, S. Kanai, J. Liu, S. Lien, H. Lowman, D. Kalonia, S. Shire, Pharm. Res. 28 (2011) 1750.
[47] V. Kumar, N. Dixit, L. Zhou, W. Fraunhofer, Int. J. Pharm. 421 (2011) 82.
[48] G. chumacher, T. van de Ven, Faraday Discuss. Chem. Soc. 83 (1987) 75.
[49] M. Tirado-Miranda, C. Haro-Pérez, M. Quesada-Pérez, J. Callejas-Fernández, R. Hidalgo-Álvarez, J. Colloid Interface Sci. 263 (2003) 74.
[50] N. Ise, I. Sogami, Structure formation in solution: Ionic polymers and colloidal particles, first ed., Springer, 2005.
[51] B. Jachimska, M. Wasilewska, Z. Adamczyk, Langmuir 24 (2008) 6866.